MORPHOLOGY OF THE LARGE-SCALE STRUCTURE

ALVARO DOMINGUEZ
Ludwig–Maximilians–Universität, Theresienstr. 37, D-80333 München, Germany
E-mail: alvaro@theorie.physik.uni-muenchen.de

The Minkowski functionals are a mathematical tool to quantify morphological features of patterns. Some applications to the matter distribution in galaxy catalogues and N-body simulations are reviewed, with an emphasis on the effects of cosmic variance. The conclusions are that (i) the observed large-scale morphology is sensitive to cosmic variance on scales much larger than the nonlinear length ($\approx 8\ h^{-1}$Mpc), and (ii) the large-scale morphology predicted by simulations is thus affected by finite-size effects, but nonetheless a ΛCDM model is favored.

1 The Minkowski functionals

The Minkowski functionals $\{M_\mu(B)\}$ are a set of morphological descriptors of the convex body B. There are $d+1$ Minkowski functionals in the d-dimensional Euclidean space (see Table 1 for the geometrical interpretation in $d = 3$). What makes these functionals interesting is that they build a *complete* set of morphological descriptors in the following sense (Hadwiger's theorem [1]): Let $M(B)$ be any functional of the bodies B in the polyconvex ring (the set of all finite unions of convex bodies) and let $M(B)$ satisfy properties (a-c) below. Then, this functional can be written as a linear combination of the Minkowski functionals. The properties to be satisfied by $M(B)$ are rather general and apparently little restrictive:

(a) Motion invariance: $M(B) = M(gB)$ (g = rotation+translation).

(b) Additivity: $M(B_1 \cup B_2) = M(B_1) + M(B_2) - M(B_1 \cap B_2)$.

(c) Convex continuity: $M(B_i) \longrightarrow M(B)$ as $B_i \longrightarrow B$ (B, B_i *convex*).

2 Cosmological applications of the Minkowski functionals

The Minkowski functionals have been only recently applied to quantify the morphological properties of the galaxy distribution [2,3]. Galaxy catalogues provide a distribution of points; a simple method to associate a body to the point distribution is the *Boolean grain model*: every point is taken to be the center of a ball of a given

Table 1. Definition of the Minkowski functionals M_μ in 3-dimensional Euclidean space

	geometric quantity	μ	M_μ
V	volume	0	V
A	surface	1	$A/8$
H	integrated surface mean curvature	2	$H/2\pi^2$
χ	Euler characteristic	3	$3\chi/4\pi$

Figure 1. The Boolean grain model with varying ball radius.

radius r, and one gets a body $\mathcal{B}_r$ formed by the union of all the balls (Fig. 1). $\mathcal{B}_r$ clearly belongs to the polyconvex ring and so Hadwiger's theorem applies.

For models of stochastic point processes, one can consider the ensemble average of the Minkowski functionals as a function of the ball radius, $\langle M_\mu \rangle(r)$. These averages depend on all the correlation functions of the stochastic process [2,4]; hence, the Minkowski functionals may be useful in cosmological investigations as a compact way for collecting information beyond the two-point level. As a matter of fact, some of the Minkowski functionals had already been employed in the cosmological literature: $\langle M_0 \rangle$ is essentially the void probability function, while $\langle M_3 \rangle$ is equivalent to the genus analysis. And the four Minkowski functionals share with these by now standard cosmological tools the robustness against errors.

A Poissonian point process (no correlations at all) provides a simple reference model for comparison, since the average Minkowski functionals can be computed analytically [5]. The shaded area in Fig. 2 represents the volume density of the average Minkowski functionals (m_μ) for this Poissonian case together with the region of 1-σ variations. For small radii, the balls barely overlap and m_μ corresponds to the Minkowski functional of an isolated ball. For large radii, the balls intersect to yield a single big body: m_0 saturates and the other m_μ become very small. The maximum in m_1 is due to the decrease in the exposed area of the balls as they start overlapping. For the same reason, m_2 has first a maximum but then becomes negative, due to the dominant negative contributions of the intersection arcs between pairs of balls. Finally, m_3 exhibits first a negative minimum due to the tunnels in the structure (negative contribution to χ), but then there is a positive maximum because of the cavities formed by the closing tunnels (positive contribution to χ).

2.1 Galaxy catalogues

Fig. 2 shows the Minkowski functionals for a volume-limited sample ($\approx 240\ h^{-1}$Mpc deep) extracted from the Abell/ACO cluster catalogue [6], containing ≈ 400 clusters. Also shown are the functionals of a Poissonian point process with the same number density. A significant deviation from the Poissonian case is observed: from the interpretation of the main features of the Poissonian curves, one concludes that this deviation describes an enhanced clustering on scales $\sim$ 15-50 h^{-1}Mpc.

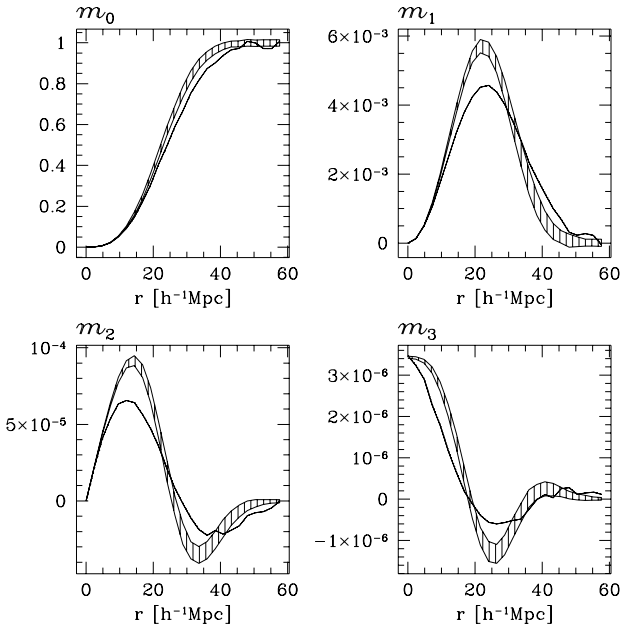

Figure 2. Minkowski functionals for the Abell/ACO cluster catalogue (solid line) and for a Poissonian point process with the same number density (shaded region, encompassing 1-σ deviations).

Fig. 3 shows the last three Minkowski functionals for a volume-limited sample ($\approx 100\ h^{-1}$Mpc deep) extracted from the PSCz galaxy catalogue [7], containing $\approx$ 1300 galaxies. The Minkowski functionals were normalized by $\langle M_1 \rangle_{\rm Poisson}$ in order to enhance the visibility. The Minkowski functionals of samples from the IRAS catalogue [8] (covering the same volume but less complete than the samples from the PSCz catalogue) exhibit the same behavior. As well as enhanced clustering, a significant deviation in the morphology between the northern and southern parts is detected. By comparing the Minkowski functionals of subsamples within the northern part and within the southern part, respectively, it could be checked that this deviation does not arise from a particular North-South anisotropy, but it is rather a signature of cosmic variance on the large scales of the sample. In fact, this variance persists when the sample depth is stretched till 200 h^{-1}Mpc.

The same kind of analysis was repeated for the CfA2 catalogue [9]. A significant deviation in the morphological features between North and South is again observed. But this conclusion is not so robust, because the sample depth, $\approx 70\ h^{-1}$Mpc, is too small: the maximum reliable ball radius is 5 h^{-1}Mpc and the results are likely dominated by local effects, as 70 h^{-1}Mpc-deep subsamples of the IRAS catalogue point out [8,9].

In conclusion, the morphological features of the galaxy distribution, as measured by the Minkowski functionals, show the effects of cosmic variance on scales larger than the "nonlinear scale" $r_0 \approx 8\ h^{-1}$Mpc (defined through $\sigma^2(r_0) = \langle \delta^2 \rangle = 1$).

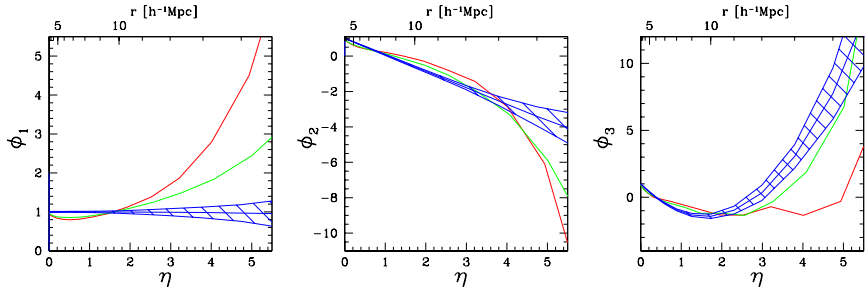

Figure 3. Minkowski functionals for the northern and southern (darker line) parts of the PSCz galaxy catalogue and for a Poissonian point process with the same number density (shaded region: 1-σ deviations). Deviations from the Poissonian case are larger for the southern part.

This must be a consequence of the sensitivity of the Minkowski functionals to correlations beyond the two-point level. In fact, they can be used to quantify the degree of planarity and filamentarity of a pattern [9,10]. So, e.g., it could be checked that galaxies in the CfA2 catalogue tend to be distributed in planar structures: this is likely a signature of the "Great Wall" and a major reason for the observed cosmic variance in this catalogue.

2.2 N-body simulations

Fig. 4 shows the Minkowski functionals extracted from cluster mock catalogues and compared with those from the Abell/ACO cluster catalogue [6]. The mock catalogues correspond to four different cosmological models (side length of the simulation box = 500 h^{-1}Mpc): standard CDM, tilted CDM (tCDM), ΛCDM, and a model with broken scale invariance (BSI) in the primordial spectrum. The deviations of the CDM and tCDM predictions from observations are larger than the estimated 1-σ dispersion (not shown) in the direction towards less clustering. The ΛCDM and BSI models fit the data much better, but they still exhibit a tendency towards less structure.

The Minkowski functionals of the CfA2 catalogue have also been compared with mock catalogues for two cosmological models: ΛCDM (box side length = 141 h^{-1}Mpc) and τCDM (box side length = 85 h^{-1}Mpc) [9]. The models predict again less clustering than observed, and, within this condition, the ΛCDM model is slightly favored.

A first conclusion is therefore the inability of the N-body simulations to reproduce the observed large-scale morphology of the galaxy distribution. Simulations systematically predict less structure than observed. A possible explanation for this result emerges when it is combined with the effects of cosmic variance mentioned in the previous subsection: the simulation volumes are too small to address the question of the large-scale morphology, so that the Minkowski functionals derived from the simulations suffer from finite-volume corrections. Within this cautionary remark, a second conclusion is that a cosmological ΛCDM model seems to provide the best fit to the observed large-scale morphology.

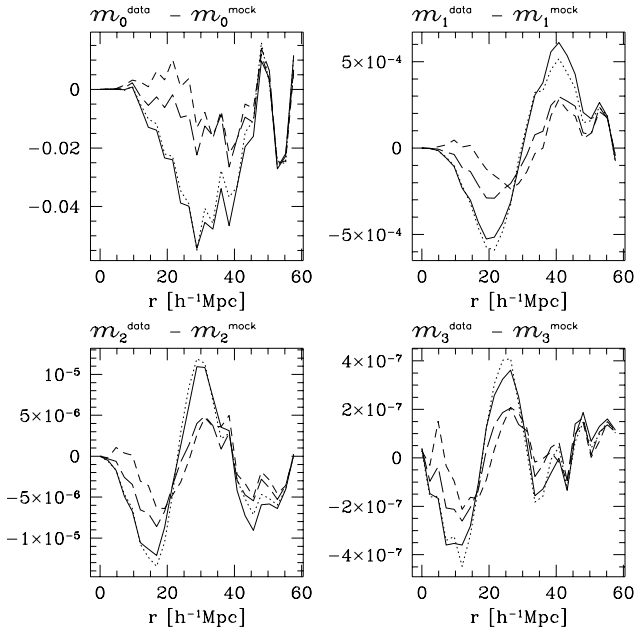

Figure 4. Difference between the Minkowski functionals of the Abell/ACO catalogue and those of mock catalogues for four cosmological models: CDM (solid), tCDM (dotted), ΛCDM (long dashed), BSI (short dashed).

Acknowledgments

The author thanks C. Beisbart, T. Buchert, M. Kerscher, J. Schmalzing and H. Wagner for their help and for permission to reproduce the figures. He also thanks the organizers for the invitation to participate in the workshop.

References

1. D. A. Klain and G.-C. Rota, *Introduction to Geometric Probability* (Cambridge University Press, Cambridge, 1997).
2. K.R. Mecke, T. Buchert and H. Wagner, *A&A* **288**, 697 (1994); astro-ph/9312028.
3. M. Kerscher in *Statistical Physics and Spatial Statistics*, eds. K. Mecke and D. Stoyan (Springer-Verlag, Heidelberg, 2000); astro-ph/9912329.
4. J. Schmalzing, S. Gottlöber, A.A. Klypin and A.V. Kravtsov, *MNRAS* **309**, 1007 (1999); astro-ph/9906475.
5. K. Mecke and H. Wagner, *J. Stat. Phys.* **64**, 843 (1991).
6. M. Kerscher et al., *MNRAS* **284**, 73 (1997); astro-ph/9606133.
7. M. Kerscher et al., *A&A*, submitted (2001); astro-ph/0101238.
8. M. Kerscher, J. Schmalzing, T. Buchert and H. Wagner, *A&A* **333**, 1 (1998); astro-ph/9704028.

9. J. Schmalzing and A. Diaferio, *MNRAS* **312**, 638 (2000); astro-ph/9910228.
10. J. Schmalzing et al., *ApJ* **526**, 568 (1999); astro-ph/9904384.